Aggregate Ramp Rates of Distributed Photovoltaic Systems in San Diego County

Mohammad Jamaly, Juan L Bosch, Jan Kleissl

***Abstract*—Aggregate ramp rates of 86 distributed photovoltaic (PV) systems installed in Southern California were analyzed and compared to irradiation measured at 5 ground stations and estimated from satellite. Irradiation data was converted to power output using a PV performance model to evaluate whether widespread on-line metering and telemetry of PV systems is necessary to track output of distributed generation for hourly resource-adequacy applications but not single or aggregated large PV systems on a distribution circuit. The satellite data were able to closely follow the aggregate power output and detect the timing of the ramps while the 5 weather stations were not as accurate due to smaller number and non-representative geographical distribution with respect to the PV sites. Over one year the largest hourly aggregate ramp was a 50% increase based on the Performance Test Conditions (PTC) rating but ramps over 30% of PTC occurred only about once per day. The effects of specific meteorological conditions, such as coastal marine layer clouds and frontal system effects, on occurrence of large ramps were investigated over the area using satellite imagery. Evaporation of morning marine layer clouds caused a disproportionally large amount of up-ramps.**

***Index Terms*-- High PV Penetration, Irradiation, Performance Model, Photovoltaic System, Ramp in Power Generation, Satellite Image.**

I. Introduction

INTEGRATION of large amounts of photovoltaic (PV) into the electricity grid poses technical challenges due to the variable power production. Solar distributed generation (DG) is often behind the meter and consequently invisible to grid operators. The ability to understand actual variability of solar DG power production will allow grid operators to better accommodate the variable electricity generation for resource adequacy considerations, such as scheduling and dispatching of power. From a system operator standpoint, it is desirable to understand when aggregate power output is subject to large ramp rates. If in a future with high PV penetration all PV power systems were to strongly increase or decrease power production simultaneously, it may lead to additional cost or even instability on the grid if the remaining generation cannot match the ramp rates and/or reserves may be exhausted. The ability to forecast such ramps can mitigate some of the economic and reliability issues [1].

[2] and [3] have analyzed output from fleets of solar DG. [2] analyzed 1-min data from 52 PV systems spread across Japan using a fluctuation index, which is the maximum difference in aggregated power output as a function of time interval. Over 1-min, sites more than about 50-100 km apart were uncorrelated. For times greater than 10-min, however, sites within 1000 km were not independent, though some of the dependence may be due to diurnal solar cycles. Analyzing output from 100 PV sites spread throughout Germany [3] found that 5-min fluctuations of ±5% of aggregate power output at rated capacity are virtually nonexistent.

In this study, performance of PV power plants installed in San Diego Gas & Electric's (SDG&E) territory is analyzed. Measured and modeled irradiation data along with power output of PV systems are applied to evaluate the frequency, magnitude, and ability to track large ramps in the aggregate power output. Since balancing areas are typically in steady state with the surrounding areas over hourly intervals, the occurrence of 1-hour large ramps is analyzed in the context of weather condition over the area. In particular mesoscale coastal marine layer clouds are investigated. Datasets are described in detail in section II. The methodology is described in section III. Results of the calculated performance model and detected largest ramps in aggregate output power are presented in section IV and conclusions are made in section V.

II. Data

The California Solar Initiative (CSI) rebate program requires a performance-based-incentive (PBI) payout for systems larger than 50 kW and makes it optional for smaller systems [4]. This requires metering and monthly submission of 15 minute energy output to the payout administrator. We have obtained the 2009 CSI measured and quality controlled [5] output for 404 PV power plants in SDG&E territory, which covers an area of 10,600 km^2. The database includes street address and various specifications of the PV systems including DC Rating (kW$_{DC}$) at standard test condition (STC), AC Rating (kW$_{AC}$) at performance test condition (PTC), module and inverter models, inverter maximum efficiency ($\eta_{Inv,\max}$), panel azimuth and tilt angles, and tracking type. The STC is the instantaneous PV system rating under controlled conditions of 1000 W m^{-2} plane-of-array irradiance, cell temperature at 25°C while the PTC is developed in an attempt to simulate real world conditions such as 1000 W m^{-2} plane-of-array irradiance, ambient air temperature at 20°C and 1 m s^{-1} wind speed. Given the rapid increase in solar DG in most coastal

This work was supported in part by the California Solar Initiative RD&D program. CSI performance data was provided by the California Center for Sustainable Energy (Timothy Treadwell). SolarAnywhere data was provided by Clean Power Research.

All authors are with the Department of Mechanical and Aerospace Engineering, University of California, San Diego 92093 USA (e-mail: smjamaly@ucsd.edu, jlbosch@ucsd.edu, and jkleissl@ucsd.edu).

urban centers in California (Los Angeles, San Francisco) which have very similar meteorological characteristics as the area in our study, this dataset presents an interesting testbed to project future effects of high PV penetration on the bulk electric grid.

The following systems were excluded from the analysis: for 74 systems only hourly averaged data was provided; 207 PV systems had more than 70% missing data, mostly because they were installed during 2009; 37 systems had more than just a single panel tilt and azimuth angle making performance calculations more challenging. Therefore, 86 PV systems with total 6.41 MW PTC rated capacity (kW_{AC}), a mean size of 74.54 kW_{AC} and median size of 6.08 kW_{AC} were analyzed (Fig. 1).

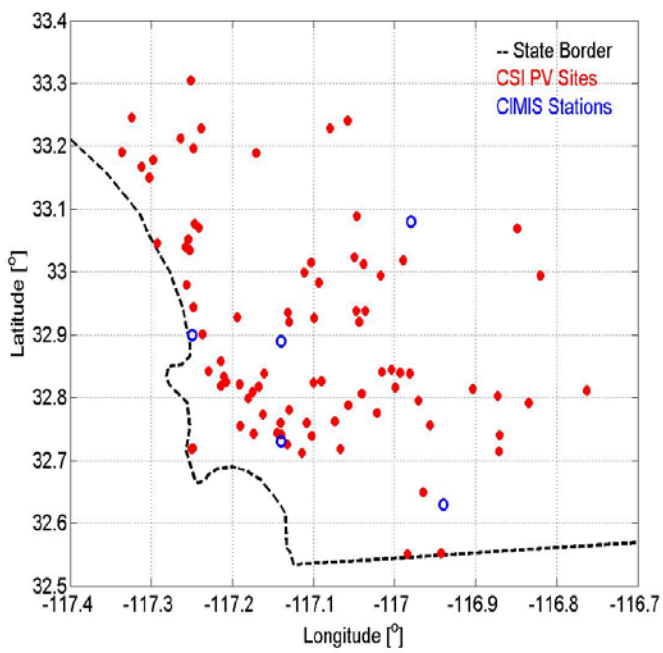

Fig. 1. Map of 86 PV systems and 5 CIMIS stations in San Diego Gas & Electric territory. The dimensions are 60 x 30 miles.

For comparison, ground measured and satellite-derived irradiation data are analyzed. Clean Power Research' commercially available SolarAnywhere (SAW) provides Global Horizontal Irradiation (GHI) and Direct Normal Irradiation (DNI) derived from Geostationary Operational Environmental Satellite (GOES) visible imagery at 1 km spatial and 30 minutes temporal resolution for California [6]. First, a cloud index is calculated from each pixel reflectance measured by the satellite. Instantaneous GHI is calculated by using the cloud index to modulate the output calculated using a clear sky model that considers local and seasonal effects of turbidity [7]. For different high quality ground measurements sites across the US, the SAW dataset was found to have root mean square error (RMSE) ranging from 77-112 W m^{-2} based on hourly average [8].

The only publicly available ground measurement data comes from the California Irrigation Management Information System (CIMIS, Fig. 1) that operates five weather stations within the study area. Hourly GHI is averaged from 60 samples by Li-Cor LI200S pyranometers with high stability silicon photovoltaic detector. These sensors are recalibrated annually resulting in typical accuracy of 3% and maximum absolute error of ±5%. Also, a three-cup anemometer (Met-One 014A; accuracy of 1.5% or 0.11 $m.s^{-1}$) and Fenwall Thermistor (Vaisala/Campbell HMP35C; accuracy of ±0.1 °C cover -24 to 48 °C range) are utilized to measure wind speed & direction and ambient temperature respectively [9].

III. Methodology

A. Performance Model

To compare SAW irradiation data for each site against the CSI measured power output, a performance model has been developed to simulate the power output. Using the GHI, DNI and tilt and azimuth angles of the PV panel, plane-of-array Global Irradiance (GI) is calculated using the Page model [10]. Besides GI, ambient air temperature and wind speed are needed to predict cell temperature (T_{cell}) which are obtained from measurements at the closest CIMIS station. The temperature efficiency correction is then calculated using a typical temperature coefficient of 0.5% K^{-1} as

$$\eta_{temp} = 1 - 0.005(T_{cell} - 25^{\circ}\mathrm{C}) \quad (1).$$

The DC power output of the PV site is estimated as

$$P_{\mathrm{mod},DC} = kW_{DC} \cdot \eta_{temp} \frac{GI}{1000\ \mathrm{Wm}^{-2}} \quad (2).$$

Inverter efficiency is modeled as [11]

$$\eta_{AC} = \frac{pf}{0.007 + 1.009\,pf + (0.0975\,pf)^2} \quad (3),$$

where the power factor is $pf = P_{\mathrm{mod},DC} / kW_{AC}$. Qualitatively, (3) is applicable for most inverters as it describes the low efficiency at small power factor, maximum efficiency at *pf* of about 0.5, and a slight decrease for larger power factors. According to the maximum inverter efficiency provided by the CSI database, $\eta_{Inv,\max}$, the calculated η_{AC} is calibrated by

$$\eta^*_{AC} = \eta_{AC} \frac{\eta_{Inv,\max}}{\max(\eta_{AC})} \quad (4),$$

where η^*_{AC} is the calibrated inverter efficiency. Next maximum power point (MPP) efficiency is considered as [12]

$$\eta_{MPP} = a_1 + a_2 GI + a_3 \ln(GI) \quad (5).$$

The MPP efficiency is applied to correct typically observed deviations in modeled output from measurements across different irradiation values using empirically obtained coefficients a_1, a_2, and a_3 [13].

Thus, the AC performance output of each site is obtained as

$$P_{\mathrm{mod},AC} = \eta_{MPP} \cdot \eta^*_{AC} \cdot P_{\mathrm{mod},DC} \quad (6).$$

To account for the rated DC efficiency at STC, line losses, and soiling, $P_{\mathrm{mod},AC}$ is calibrated by the ratio of the annual average CSI measured to modeled power output.

$$P^*_{\mathrm{mod},AC} = P_{\mathrm{mod},AC} \frac{avg(P_{measured})}{avg(P_{\mathrm{mod},AC})} \quad (7),$$

where $P^*_{\mathrm{mod},AC}$ is the calibrated modeled AC output power. The calibration guarantees that modeled averaged annual

performance based on SAW irradiation is consistent (or without bias) with observed performance. Such a 'modeled output statistics (MOS)' correction would typically also be applied in operational forecasting of PV power output.

B. *Largest Aggregate PV Ramp Rates*

The objective of the ramp rate analysis is two-fold. Firstly, knowledge about the largest possible aggregate ramp rates and underlying meteorological conditions is useful for system operators. Secondly, under extreme ramp rate conditions, knowing the PV output in real time would be most valuable since ISO regulation up or regulation down capacity would be used up or have to be quickly procured. The ability of CIMIS and SAW modeled PV performance to match actual output is therefore of interest.

The aggregate CSI measured power output for the 86 PV systems in 2009 is used to determine the largest ramp rates. We present normalized ramp rates to facilitate scaling the results to future PV penetration scenarios; the aggregate power outputs are normalized by the aggregate kW_{AC} capacity of the PV systems for each time period (Figs. 3, 4). Also to facilitate the comparison between CIMIS, SAW, and CSI, the aggregate power outputs and aggregate measured GHI at 5 CIMIS stations are normalized by the respective maximum daily values (normalized to a maximum of 1 for each day in Figs. 6, 8).

IV. Results

A. *Performance Model*

Modeled power output (derived from SAW irradiation) is calculated from (7) and compared to measured power output for all 86 PV systems (Fig. 2). The average calibration factor of 0.937, the ratio of annual average of $P_{measured}$ to $P_{mod,\,AC}$ in (7), confirms that the performance model generally overestimates, likely due to line losses and soiling of the PV systems that are not considered in (6). Typical differences (as measured by the MAE and RMSE) between the modeled and measured performance are 15 to 20% for 30-min averaged data.

Dependencies of the error in modeled performance on cell temperature, ambient temperature, wind speed, zenith angle, and inverter efficiency were examined. However, no trend in the error was found (not shown) indicating that a more complex model for these variables would not necessarily improve the agreement. The remaining discrepancy seems to be related to inaccuracy in the SolarAnywhere irradiance mostly due to location errors in the cloud fields due to satellite navigation errors and cloud-to-shadow parallax.

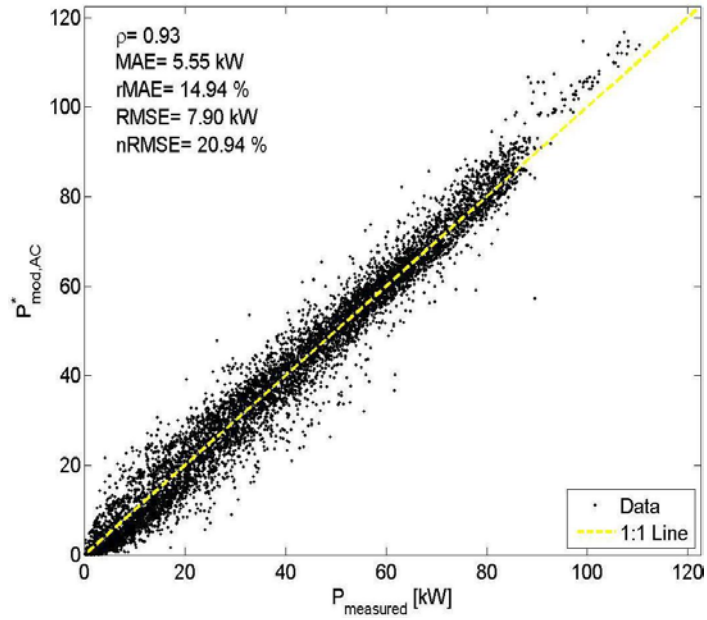

Fig. 2. Calibrated SAW performance, (7) with 30-min time step, versus CSI measured output (averaged over two 15-min time steps), averaged over the 86 PV sites shown in Fig. 1. The yellow line is the 1:1 line which would indicate perfect agreement between the datasets. The caption indicates correlation coefficient (ρ), mean absolute error (MAE), relative MAE, root mean square error (RMSE), and relative RMSE between the datasets. rMAE and rRMSE are normalized by annual average of the measured output data.

B. *Large Hourly Ramps in Aggregate Output*

The largest ramp rates in the aggregate measured PV output (normalized by kW_{AC}) are detected over the year for different intervals (Fig. 3). As expected, the maximum ramp rate / step size increases with the ramp interval. The increase is near linear up to about 105 minutes at about 0.6% of PTC per minute and then levels off as the maximum possible step size of 1 is approached. The largest up-ramps are slightly larger than the largest down ramps indicating that cloudy to clear transitions are driven by faster moving clouds and/or a larger rate of change in atmospheric optical depth.

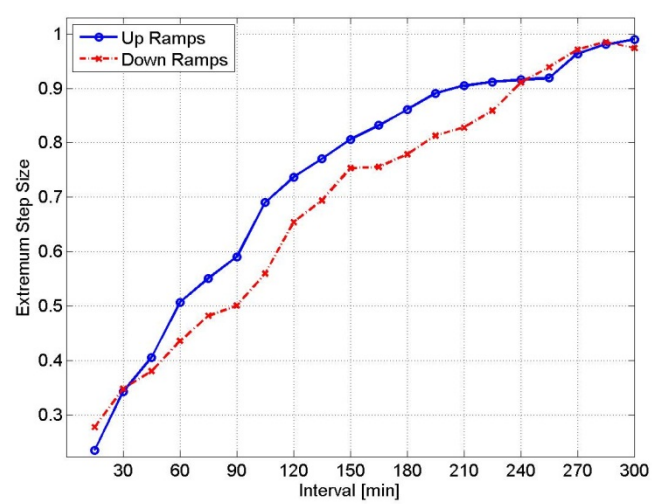

Fig. 3. Largest step size ($P_{measured}/kW_{AC}$) versus ramp time interval (from 15-min up to 5-hours) for the aggregate output from 86 PV sites in 2009.

1-hour ramp rates have a special significance as most energy exchange between electric balancing areas is scheduled over hourly intervals. The distribution of 1-hour ramp rates in the normalized aggregate measured PV output (Fig. 4) shows that ramps over 25% hr^{-1} of PTC capacity are relatively rare. Below that the distribution decreases linearly. Presumably this is due to the fact that the very large ramps are caused by coincident increase or decrease in both cloudiness and solar zenith angle which is unlikely. Smaller ramps are simply caused by the diurnal cycle of irradiance in the typically mostly clear conditions in the area.

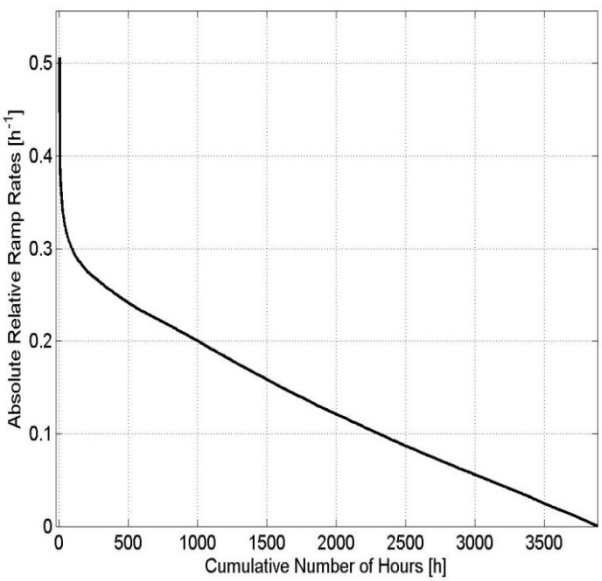

Fig. 4. Cumulative distribution of absolute value of 1-hour ramp rates of normalized aggregate 15-minute PV output from all 86 PV sites in 2009. The ramps are zero for the remaining hours up to 8760 h, because these are night time conditions.

Fig. 5 shows a histogram of the 1-hour ramp rates larger than 30% of PV capacity by month. During the summer months ramps are most likely caused by marine layer overcast cloud breakup. On the other hand, ramps occurring during the winter months are related to storm systems moving into (large down ramp) or out of the area (large up-ramp). Large ramps were more likely in the spring and summer months (with the exception of July) when they occurred about every day. Presumably this is due to the marine layer cloud evaporation in the morning coincident with increasing solar altitude angle and amplified by the large irradiation in these months (due to larger solar altitudes compared to winter months). Large ramps are not correlated with average output over a month; for example July with the largest PV output actually had the least large ramps.

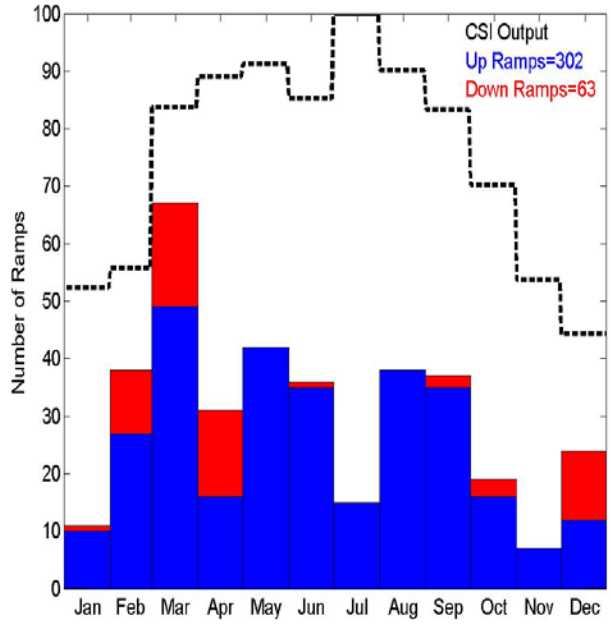

Fig. 5. Histogram of the largest 1-hour ramp rates (30% and larger) of normalized aggregate 15-minute PV output from all 86 PV sites in 2009 by month. The black line shows percentage of the measured aggregate 15-minute PV output from all 86 PV sites normalized to the maximum month (July).

Fig. 6 shows daily profiles of the normalized aggregate CSI measured and SAW modeled power outputs along with the normalized aggregate CIMIS GHI (all normalized to a maximum of 1 as described in Section III. B) for the days when the four largest ramps were observed. The largest ramps caused a change of 50.6% expressed in PTC capacity within one hour while the next 3 largest ramps were only 44%. SAW estimates tracked the CSI power output typically within 6% rMAE at 30-min resolution. The only exception was Nov 29 with a 12% MAE due to a positive bias by the satellite in the afternoon. SAW matched the magnitude and timing of the ramps accurately. The CIMIS stations are at a disadvantage as only 5 stations exist that are not spatially distributed like the CSI sites and only have hourly data. Due to the hourly averaging the ramp magnitudes are underestimated by CIMIS. The rMAE differences for CIMIS are about twice those for SAW.

The 30 minute consecutive GOES images for the time period with the largest ramp (Fig. 6a), are illustrated in Fig. 7. At first it appears to be a typical summer morning with coastal overcast stratus. However, detailed investigation shows unusual clear conditions along the coast with broken clouds inland centered over the area with the most PV systems. The clouds rapidly evaporate between 900 and 1000 PST causing a large up-ramp.

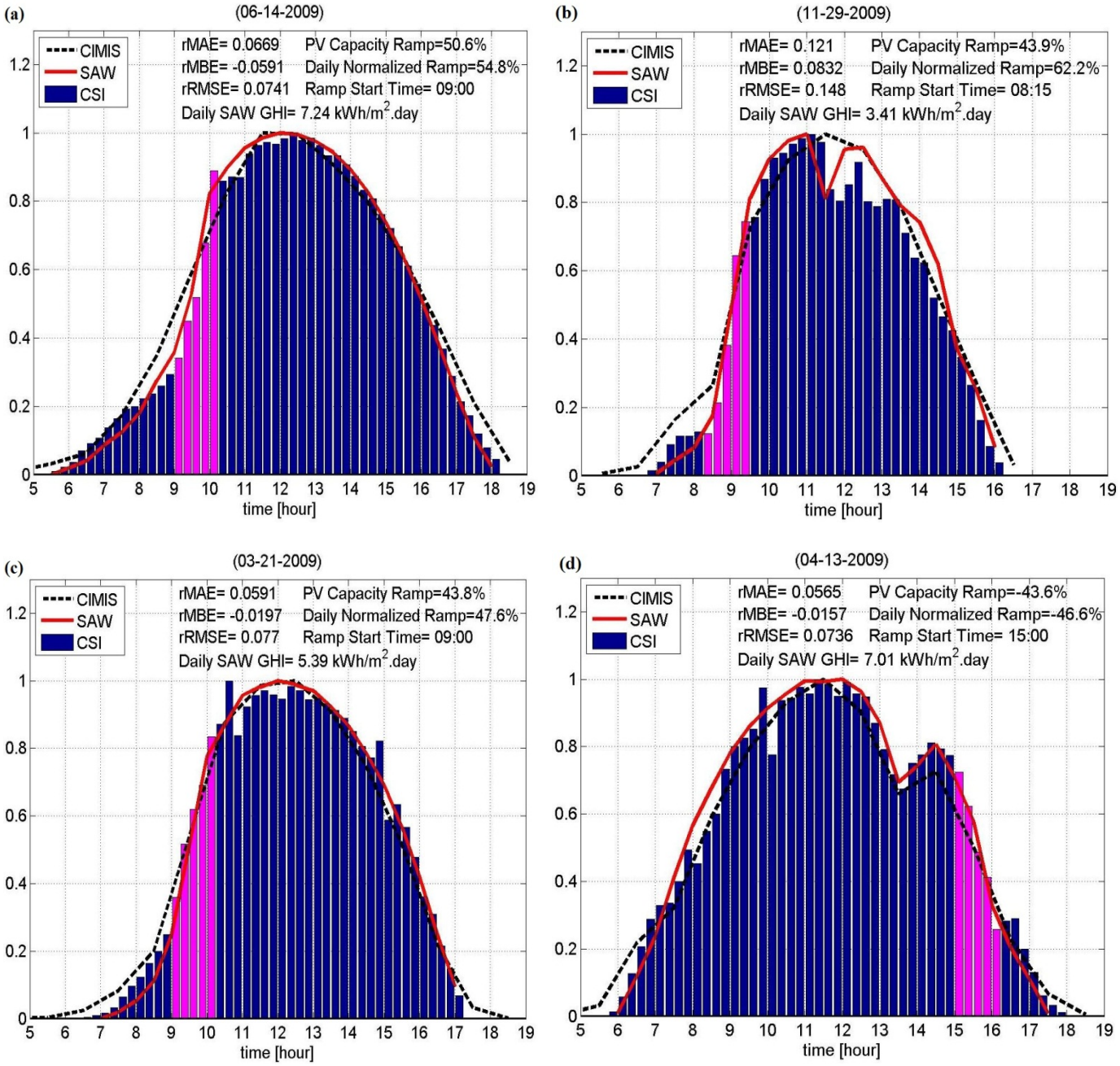

Fig. 6. Normalized aggregate 15-minute PV output from all 86 PV sites for the days with the largest 1-hour ramp rates in 2009 (bars). Magenta colors show the timing of the large ramp and the caption indicates the daily available GHI from SolarAnywhere database (averaged over the locations of the 86 PV sites), the ramp magnitudes (normalized by both PV PTC capacity and daily maximum output) and timing of the ramp. Normalized aggregate 30-minute performance output of these sites obtained from SolarAnywhere satellite based irradiance at each pixel (red) and normalized aggregate hourly measured GHI of 5 weather stations (black) are also shown. Relative (divided by annual average CSI output) mean absolute error (MAE), mean bias error (MBE), and RMSE between normalized aggregate SAW performance and CSI outputs are presented for each day as well. (a) Jun. 14, 2009, (b) Nov. 29, 2009, (c) Mar. 21, 2009, (d) Apr. 13, 2009.

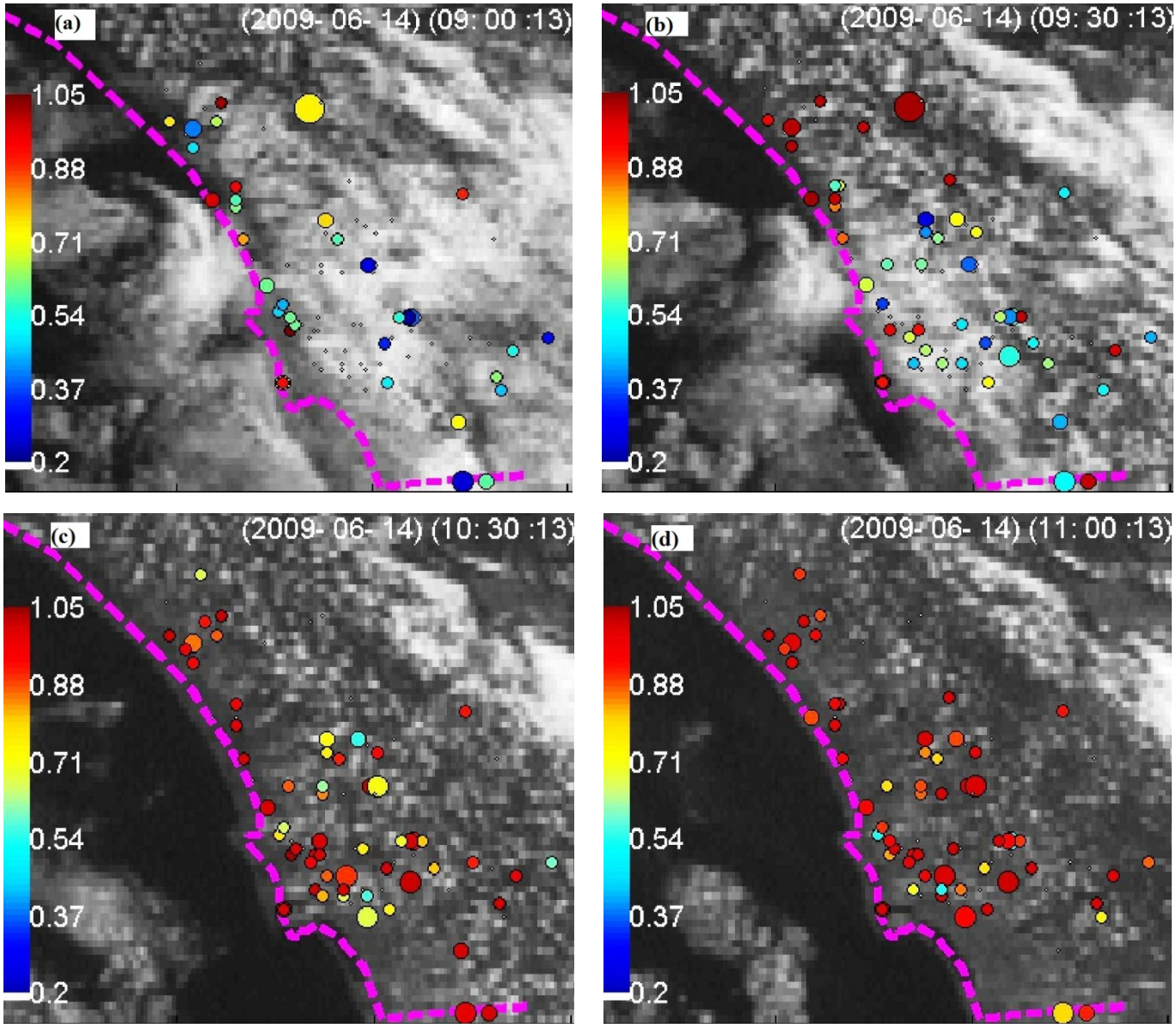

Fig. 7. GOES satellite images at 30 minute resolution on Jun. 14, 2009 (Fig. 6a). The circles represent 86 PV systems shown in Fig. 1. The area of the circles is proportional to the power rating of the PV system (the largest system is 939 kW) and the color bar shows ratio of 15-min averaged output to annual maximum output at that time of day (ToD). (a) 900, (b) 930, (c) 1030, and (d) 1100 PST. The largest aggregated 1 hour ramp for this period was 50.6% of PV capacity and occurred from 900 to 1000 PST.

While the four most extreme hourly ramps occurred in a variety of season due to unique weather conditions with fast moving and/or evaporating / forming clouds, in Fig. 5 we had demonstrated that most of the largest hourly ramps of aggregate PV output occur in the summer months. Further investigation (not shown) revealed that marine layer breakup caused most of these ramps motivating further analysis of one exemplary day, June 24 (Fig. 8). The 30 minute consecutive GOES images for a time period with marine layer cloud breakup are illustrated in Fig. 8. A large morning up-ramp (38.1% of installed PV capacity per hour) occurred due to marine layer retreat that occurs over 3 hours (7:30am-10:30am). While the cloudiness on June 24 is more widespread and overcast, the ramp rate is smaller than on June 14 since the marine layer retreat occurs over several hours reducing the ramp rate.

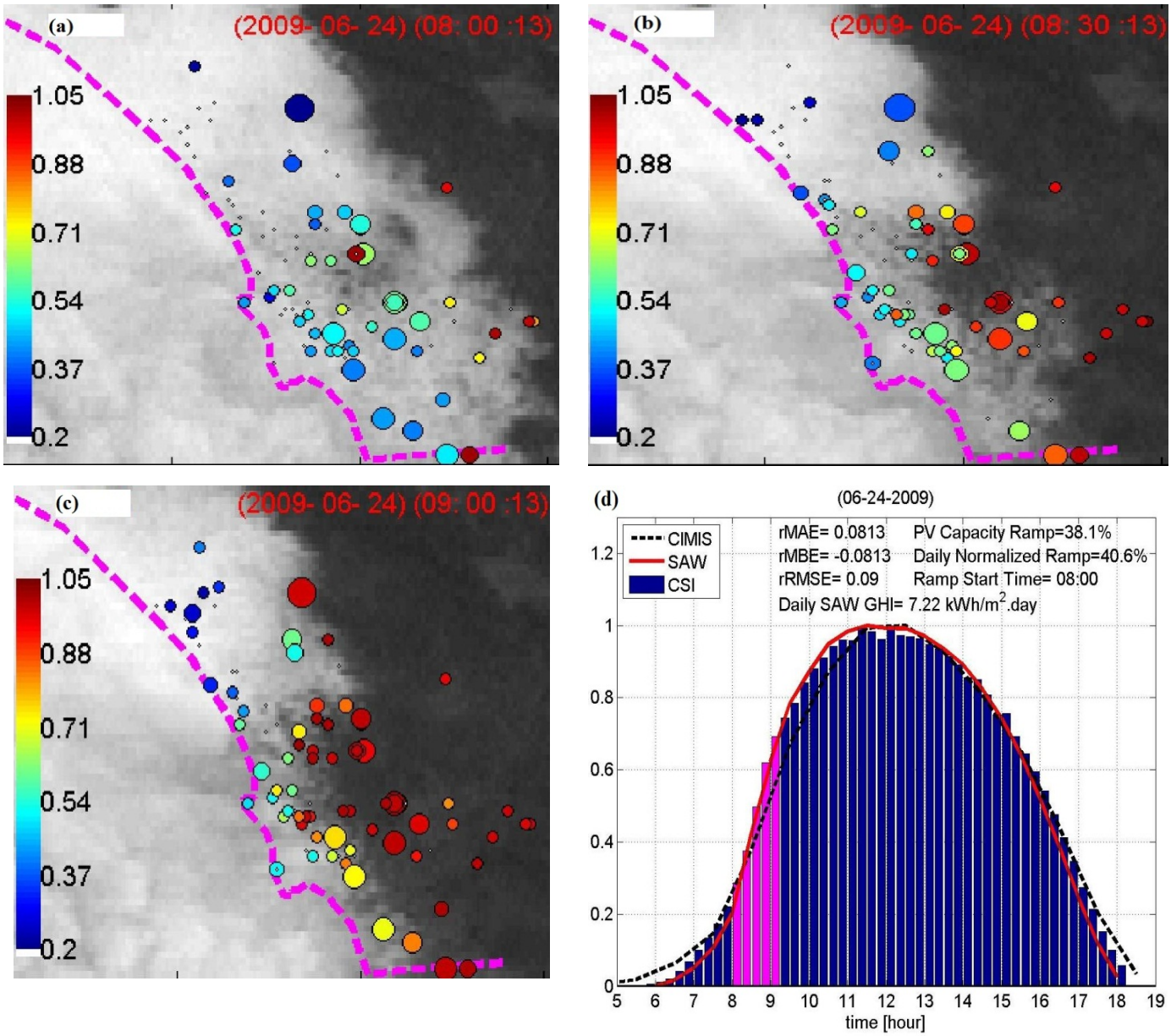

Fig. 8. GOES satellite images at 30 minute resolution on Jun. 24, 2009 showing a transition from marine layer overcast stratus to clear from 800-0900 PST. The circles represent 86 PV systems shown in Fig. 1. The area of the circles is proportional to the power rating of the PV system (the largest system is 939 kW) and the color bar shows ratio of 15-min averaged output to annual maximum output at that time of day (ToD). (a) 800, (b) 830, (c) 900. d) The largest aggregated 1 hour ramp for this period was 38.1% of PV PTC capacity (occurred 800-900 PST). See caption of Fig. 6 for details.

V. Conclusion

Aggregate power output of 86 PV systems in Southern California was presented and compared to satellite-derived Solar Anywhere irradiation and measured GHI at five weather stations (CIMIS). A PV performance model was developed to calculate the expected power output for each PV system from irradiation data. An average PV solar conversion efficiency of 16% ($\eta^{*}_{AC} \cdot \eta_{temp}$, at maximum power point) resulted in the best agreement with the power output measurements.

The main focus was on detecting the largest ramps in PV output over the year. It was encouraging that the PV performance model applied to the satellite data was able to follow the power output measured over 86 systems typically within 6% during the four largest ramps. The satellite data also matched the timing of the ramps accurately while the weather stations were not as accurate due to smaller number and non-representative geographical distribution with respect to the PV sites. During the extreme ramps, the ability to estimate PV output in real time would be most valuable since regulation up or regulation down capacity would be used up or have to be quickly procured.

The largest hourly ramp was 50.6% of PTC capacity followed by several ramps of up to 44% of PTC capacity. In a very high PV penetration scenario, if such ramps hit the operator unprepared, they would indeed cause problems on the grid and require curtailment of demand or supply. However,

solar forecasting can alert the operator to potential contingency conditions a day or at least a few hours ahead. Since maximum ramp rates during intervals shorter than 1 hour decrease about linearly with time interval, short term aggregate ramp rates are relatively benign at about 0.6% per minute. However, the analysis does not apply to single PV systems, which will show much larger short-term ramp rates that – in extreme cases - can result in exceedance of voltage tolerance bands on distribution feeders.

Not the most extreme ramps, but many of the largest ramp rates of aggregate PV output in SDG&E territory are caused by summer marine layer breakup when cloud evaporation coincides with an increase in solar altitude nearly every morning. During the winter months, the ramp rates are mainly caused by the winter frontal storm systems; when fast-moving storm systems move into (large down ramp) or out of the area (large up-ramp). However, the generally smaller solar altitude, low probability of frontal passages and their randomness with respect to time of day caused overall less large ramps during the winter. In terms of solar forecasting, for the day-ahead market frontal passages can be forecast more accurately than especially the timing of marine layer events. Development and improvement of solar forecast models should focus on the latter events.

VI. Acknowledgments

We acknowledge (i) funding and data from the California Public Utilities Commission California Solar Initiative RD&D program, (ii) Jennifer Luoma for reading in the data, (iii) Timothy Treadwell from the California Center for Sustainable Energy for providing the 2009 SDG&E CSI data, (iv) Stephan Barsun (Itron) for helpful discussions on data quality control.

VII. References

[1] P. Bacher, H. Madsen, and H. A. Nielsen, "Online short-term solar power forecasting," Solar Energy, 83:1772-1783, 2009.

[2] A. Murata, H. Yamaguchi, and K. Otani, "A Method of Estimating the Output Fluctuation of Many Photovoltaic Power Generation Systems Dispersed in a Wide Area," Electrical Engineering in Japan, 166(4), 2009.

[3] E. Wiemken , H. G. Beyer, W. Heydenreich, and K. Kiefer, "Power Characteristics Of PV Ensembles: Experiences from the Combined Power Production Of 100 Grid Connected PV Systems Distributed Over The Area Of Germany," Solar Energy, 70(6):513–518, 2001.

[4] California Solar Initiative, "California Public Utilities Commission California Solar Initiative Program Handbook," Accessed Sep. 2011 at: http://www.gosolarcalifornia.org/documents/CSI_HANDBOOK.PDF

[5] Itron, Inc. & KEMA, Inc., "CPUC California Solar Initiative 2009 Impact Evaluation," Jun. 2010. Available: http://www.cpuc.ca.gov/NR/rdonlyres/70B3F447-ADF5-48D3-8DF0-5DCE0E9DD09E/0/2009_CSI_Impact_Report.pdf

[6] Web-based Clean Power Research service database, SolarAnywhere. Available: https://www.solaranywhere.com/Public/About.aspx

[7] Perez, R., Ineichen, P., Moore, K., Kmiecik, M., Chain, C., George, R., and Vignola, F., "A new operational model for satellite-derived irradiances: Description and validation," Solar Energy, 73(5):307-317, 2002.

[8] Perez, R., Kivalov, S., Schlemmer, J., Hemker, K., Renné, D., and Hoff, T., "Validation of short and medium term operational solar radiation forecasts in the US," Solar Energy, 84(12):2161-2172, 2010.

[9] CIMIS Sensor Specifications. Accessed on Dec 1 2011 at: http://wwwcimis.water.ca.gov/cimis/infoStnSensorSpec.jsp

[10] J. Page, The Role of Solar Radiation Climatology in the Design of Photovoltaic Systems, in: T. Markvart, L. Castaner, Practical Handbook of Photovoltaics: Fundamentals and Applications, Elsevier, Oxford, 2003, pp. 5-66.

[11] J. Luoma, J. Kleissl, and K. Murray, "Optimal Inverter Sizing Considering Cloud Enhancement," Solar Energy, 86(1): 421-429, 2012.

[12] S.R. Williams, T.R. Betts, T. Helf, R. Gottschalg, H.G. Beyer, and D.G. Infield, "Modelling Long-Term Module Performance based on Realistic Reporting Conditions with Consideration to Spectral Effects," 3rd World Conference on Photovoltaic Energy Conversion, Osaka, Japan, May 11-18, 2003.

[13] H.G. Beyer, J. Betcke, A. Drews, D. Heinemann, E. Lorenz, G. Heilscher, and S. Bofinger, S, "Identification of a General Model for the MPP Performance of PV-Modules for the Application in a Procedure for the Performance Check of Grid Connected Systems," 19th European Photovoltaic Solar Energy Conference and Exhibition, Paris, France, 07.06.-11.6.2004, pp3073-3076.